Expanded View Figures

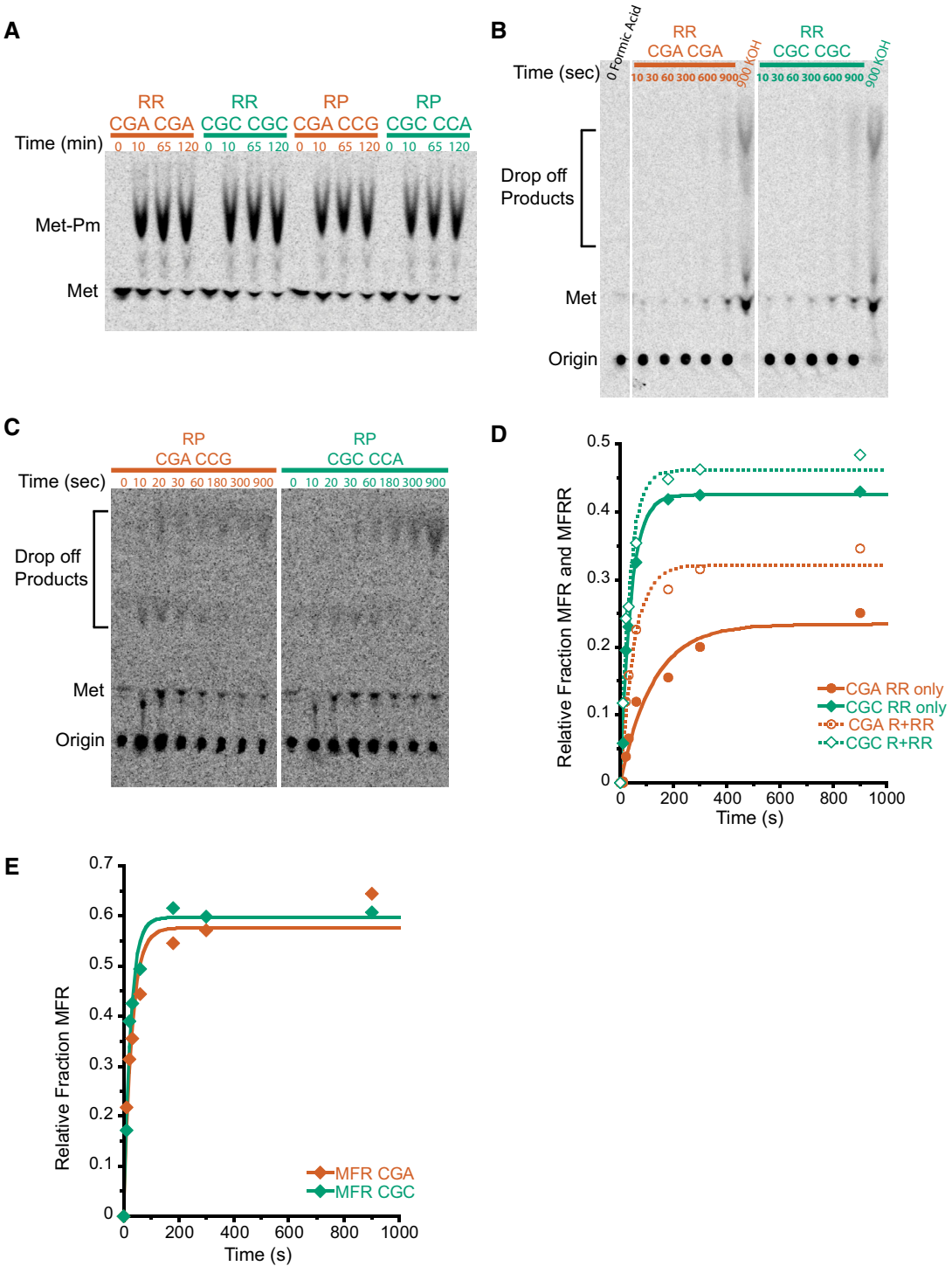

Figure EV1.

Figure EV1. Initiation complex test of Met–Pm activity and individual product analysis of MFRR elongation.

A Met–Pm activity for all the ICs formed with WT ribosomes on inhibitory mRNAs (red) and optimal mRNAs (green). There is no significant difference in activity at the last time point for any of the ICs.

B TLC showing peptidyl-tRNA drop-off using the PTH assay on MFRR ICs with the inhibitory (CGA–CGA) pair (red) and the optimal (CGC–CGC) pair (green). Time points were quenched with formic acid to assess drop-off, and time points quenched with KOH were to monitor peptide formation as a control. There is no significant accumulation of peptidyl-tRNA drop-off products.

C TLC showing peptidyl-tRNA drop-off using the PTH assay on MRPK ICs with the inhibitory (CGA–CCG) pair (red) and the optimal (CGC–CCA) pair (green). Time points were quenched with formic acid to assess drop-off. There is no significant accumulation of peptidyl-tRNA drop-off products.

D Elongation kinetics for the MFR and MFRR products together versus the final MFRR product alone for the inhibitory (CGA–CGA) pair (red) and the optimal (CGC–CGC) pair (green). The increased rate and amount of product formed for the MFR and MFRR data compared to the MFRR alone suggest that the addition of the second arginine is slower than the first.

E Elongation kinetics for the addition of a single arginine on an MFR (CGA) message in red and MFR (CGC) message in green. The addition of the first arginine is similar for CGA and CGC, again suggesting that the addition of the second arginine is the slower step.

Figure EV2. tRNA concentration titration and replicates with statistical analysis for UCG exact match tRNA experiments.

A Titration of aa-tRNA to establish high concentration as saturating for elongation experiments. With this system, it is difficult to increase tRNA concentration, but going only twofold lower in concentration, we do not see differences in the amount of full-length MFRR product being formed at early (60 s) time points as shown by the quantification below the TLC.

B Comparison of observed rates of elongation for inhibitory CGA–CGA codon pair decoded by the native arginine ^{ICG}tRNA (red), inhibitory CGA–CGA codon pair decoded by the non-natural arginine ^{UCG}tRNA (pink), and the optimal CGC–CGC codon pair decoded by the native arginine ^{ICG}tRNA (green). Data from experiments performed with limiting tRNA concentrations shown in hatched bars (25 nM aa-tRNA) and saturating tRNA concentrations in solid bars (250 nM aa-tRNA). Error bars represent standard deviations calculated from at least three experimental replicates (exact number of replicates indicated by the number of dots for each bar plotting the mean for the data). *P*-values calculated using Student's *t*-test and rounded to two decimal places.

C Comparison of observed endpoints for inhibitory CGA–CGA codon pair decoded by the native arginine ^{ICG}tRNA (red), inhibitory CGA–CGA codon pair decoded by the non-natural arginine ^{UCG}tRNA (pink), and the optimal CGC–CGC codon pair decoded by the native arginine ^{ICG}tRNA (green). Data from experiments performed with limiting tRNA concentrations shown in hatched bars (25 nM aa-tRNA) and saturating tRNA concentrations in solid bars (250 nM aa-tRNA). Error bars represent standard deviations calculated from at least three experimental replicates (exact number of replicates indicated by the number of dots for each bar plotting the mean for the data). *P*-values calculated using Student's *t*-test and rounded to two decimal places.

D–F Elongation kinetics for the CGA–CGA inhibitory codon pair with the native arginine ^{ICG}tRNA (red) or the non-native arginine ^{UCG}tRNA (pink) and for the CGC–CGC optimal control pair with the native arginine ^{ICG}tRNA (green) for the three other replicate experiments used to calculate the averages in (B and C).

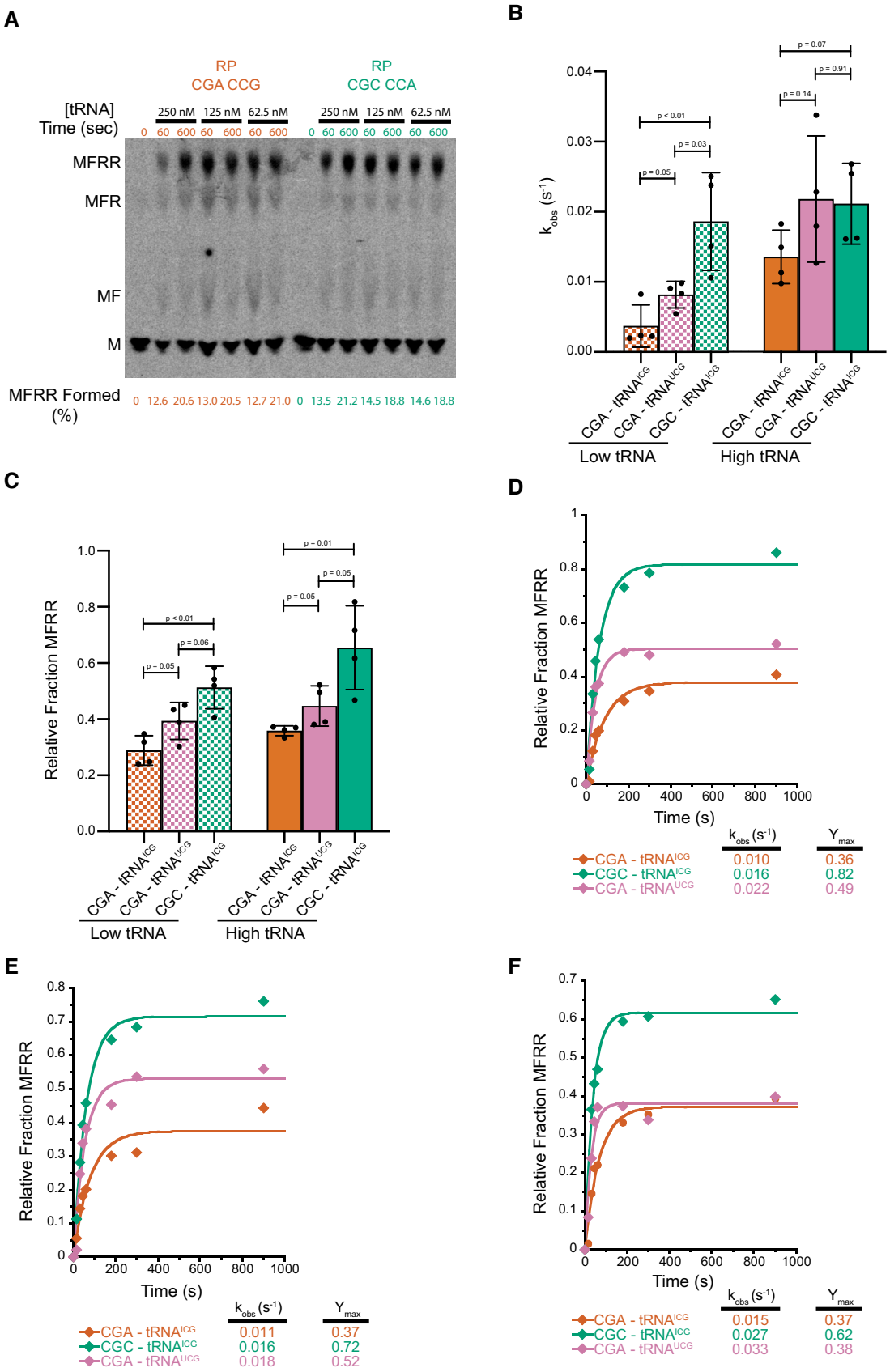

Figure EV2.

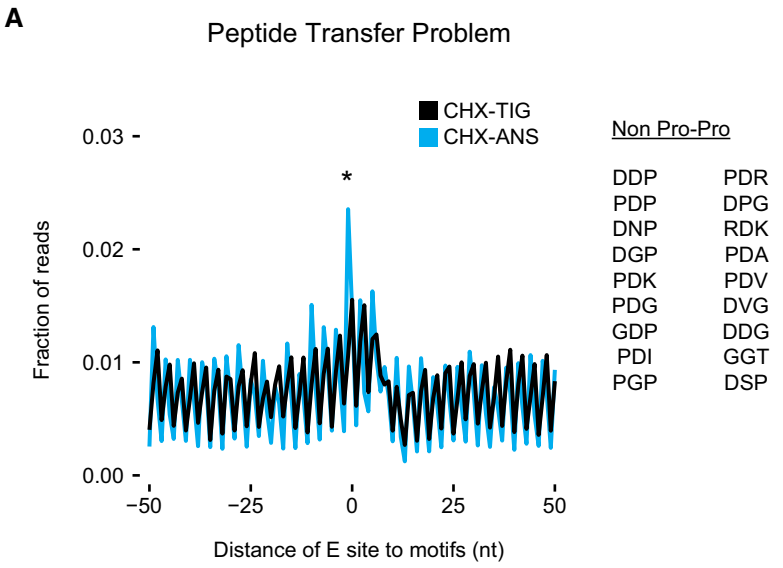

Figure EV3. Ribosome profiling analysis showing defects in peptide bond formation.
Metacodon analysis of 21-nt RPFs in libraries prepared with CHX/ANS (blue) showing an increase in ribosome density at tripeptide motifs that undergo slow peptide bond formation (Schuller *et al*, 2017) compared to libraries prepared with CHX/TIG. *P*-value was determined by Student's *t*-test between CHX-TIG and CHX-ANS datasets on the tripeptide motifs indicated (**P* = 0.0363, *n* = 3).

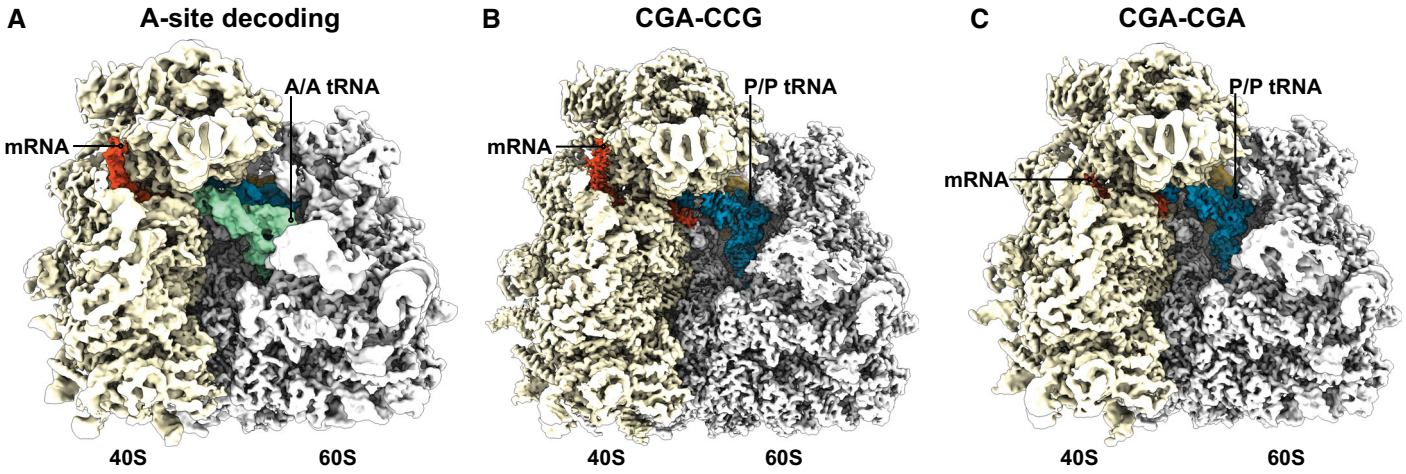

Figure EV4. Cryo-EM structures of RNCs stalled on inhibitory codon pairs in comparison with the A-site decoding situation.

A–C Cryo-EM density maps filtered according to local resolution used to build molecular models. (A) Cryo-EM map of the pre-state RNC with tRNA in the A site. (B) Cryo-EM map of the CGA–CCG-stalled RNC. (C) Cryo-EM map of the CGA–CGA-stalled RNC.

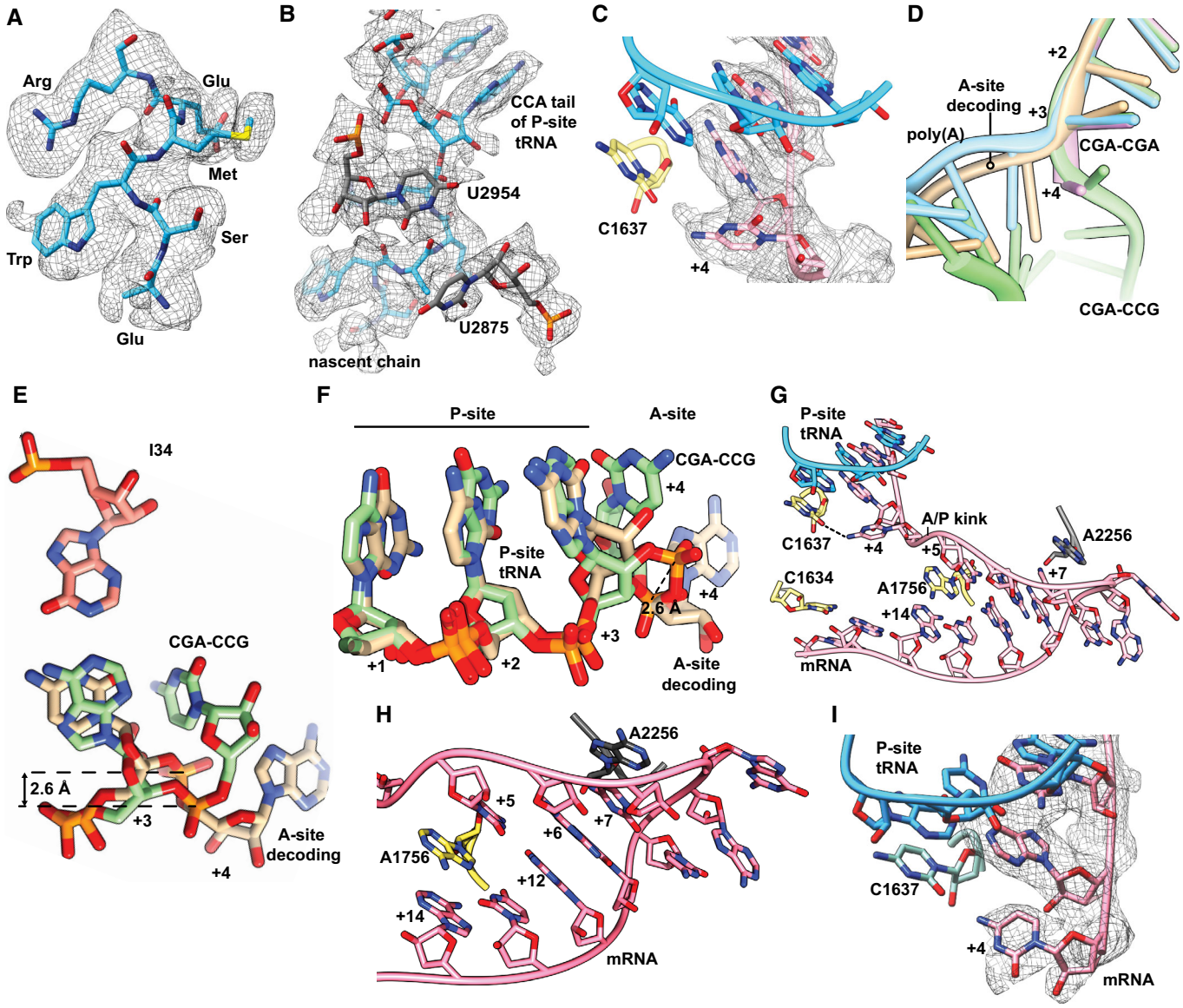

Figure EV5. Structural details of the codon-based stalling.

A Cryo-EM density (mesh) and stick model of the nascent chain residues modeled in the 80S ribosome stalled on the CGA–CCG inhibitory codon pair. The density of the CGA-encoded Arg of the first codon pair is clearly distinguishable as well as the bulky density of Trp_{65} of the uL4 encoded upstream in the translated mRNA construct.

B Cryo-EM density (mesh) and stick model of the peptidyl-transferase center as observed in the structure of ribosome stalled on the CGA–CCG inhibitory codon pair. Notably, for the U2875 (U2506 in *E. coli*), no clear density is observed, most likely due to enhanced flexibility. Yet, no directly observable major perturbation of the PTC components is apparent.

C Cryo-EM density (mesh) and stick model with cartoon phosphate backbone representing the mRNA positions +1 to +4 and their interactions in the CGA–CCG-stalled ribosome.

D Effect of flipped C+4 on the general path of the mRNA in the A site. A cartoon representation of mRNAs in all four discussed 80S structures is compared.

E, F Comparison between the A-site tRNA decoding situation and the CGA–CCG-stalled situation of the mRNA in positions +1 to +4. In the CGA–CCG A site, the C+4 is flipped by approximately 95° degrees toward the wobble A:I base pair and the mRNA backbone is shifted by 2.6 Å at the phosphate linking A+3 and C+4.

G Overview of the mRNA and its interactions in the A site of CGA–CCG reporter stalled ribosome using stick model with cartoon phosphate backbone representation. Sequence of mRNA positions +4 to +14 is CCGCGACCGUA.

H Detail of the tip of the hairpin from (G) with stabilizing stacking interactions between A2256 of the 25S rRNA and the C+7 of the mRNA and among A1756 of the 18S rRNA intercalated between the C+5 and the A+14 of the mRNA.

I Cryo-EM density (mesh) and stick model with cartoon phosphate backbone representing the mRNA positions +1 to +4 and their interactions in the CGA–CGA-stalled ribosome.

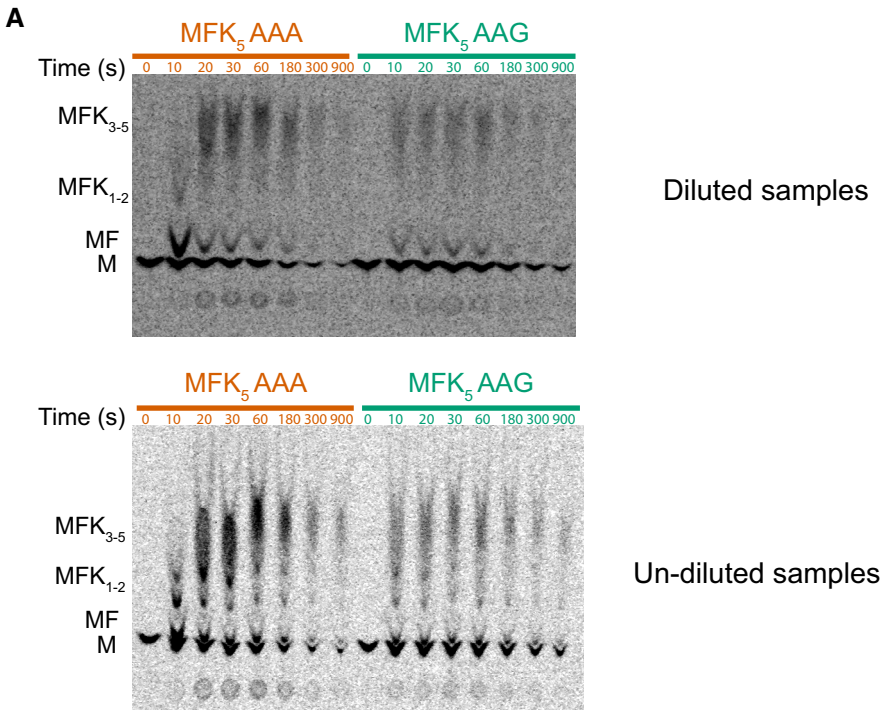

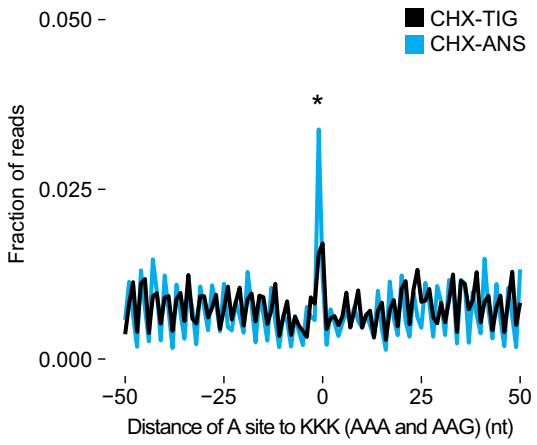

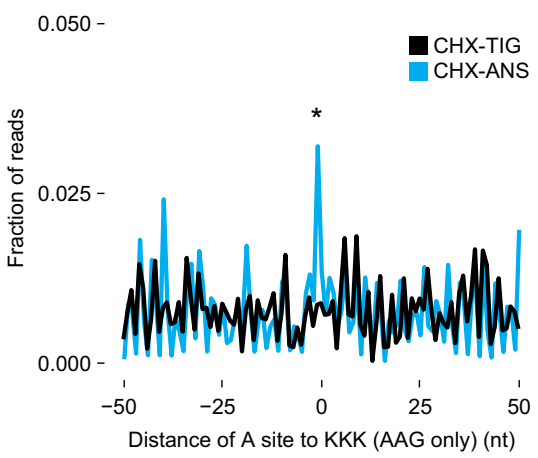

Figure EV6. Elongation of AAA is slower than AAG on MFK_5 initiation complexes.

A TLC showing peptide bond formation of MFK_5 messages on inhibitory AAA codons (red) and control AAG codons (green). Samples were diluted 1–4 μl in water (top) or undiluted (bottom) to better resolve individual products on TLC. MFK_5 AAG complexes are making longer lysine peptides (indicated by higher bands on the TLC) than AAA at early time points.

B Metacodon analysis of 21-nt RPFs in libraries prepared with CHX/ANS (blue) and CHX-TIG (black) showing an increase in ribosome density at polylysine motifs (KKK) comprised of both AAA and AAG codons. *P*-value was determined by Student's *t*-test between CHX-TIG and CHX-ANS datasets on the tripeptide motifs indicated (*P = 0.0204, n = 3).

C Metacodon analysis of 21-nt RPFs in libraries prepared with CHX/ANS (blue) showing an increase in ribosome density at polylysine motifs (KKK) comprised of only AAG codons indicative of slow peptide transfer compared to libraries prepared with CHX-TIG (black). *P*-value was determined by Student's *t*-test between CHX-TIG and CHX-ANS datasets on the tripeptide motifs indicated (*P = 0.0117, n = 3).